Hindawi
Advances in Materials Science and Engineering
Volume 2022, Article ID 5302142, 15 pages
https://doi.org/10.1155/2022/5302142

*Research Article*

# Research and Evaluation on Dynamic Response Characteristics of Various Pavement Structures

**Meng Guo**[1], **Fujin Hou**[2], **Shuaixiang Zhang**[1], **Xu Li**[3], **Yunliang Li**[3] and **Yufeng Bi**[4]

[1]*The Key Laboratory of Urban Security and Disaster Engineering of Ministry of Education, Beijing University of Technology, Beijing 100124, China*
[2]*Shandong Hi-Speed Construction Management Group Co. Ltd, Jinan 250001, China*
[3]*School of Transportation Science and Engineering, Harbin Institute of Technology, Harbin 150090, China*
[4]*Shandong Provincial Communications Planning and Design Institute Group Co. Ltd, Jinan 250101, China*

Correspondence should be addressed to Shuaixiang Zhang; zhangsx@emails.bjut.edu.cn

Received 18 November 2021; Accepted 15 February 2022; Published 11 March 2022

Academic Editor: Abílio De Jesus



In order to comprehensively analyze the dynamic response of full-depth asphalt pavement under moving load, a three-dimensional model of pavement structure and dynamic load moving zone are established based on ABAQUS finite element software. Based on the time history curves of different structures, the stress-strain states at the bottom of each structural layer in different structures under moving load are analyzed. The results show that the stress, strain, and shear stress of the middle layer of full-depth pavement are smaller than those of semirigid base pavement, and rutting is closely related to the deformation of this layer. The dynamic response results of the same structure at different speeds are similar, but the increase of the maximum speed will increase the shear stress at the bottom of the layer, and the road is more prone to longitudinal crack.

## 1. Introduction

In recent years, in order to deal with various overload and heavy load pavement conditions in the future, more and more countries begin to study the design and use of asphalt stabilized macadam flexible base in permanent roads, and the full-depth pavement structure has attracted a lot of attention. This kind of pavement can deal with road cracks and other problems depth by easily and quickly treating the surface wearing course. It does not need large-scale repair in the process of realizing the service function for a long time [1–3] and has its unique advantages in combating the reduction of service life caused by fatigue [4, 5].

In the design method of semirigid base course pavement based on classical pavement structure, the design method of the static load instead of vehicle dynamic load cannot reflect the real-time stress state of pavement structure, resulting in cracks, pits, ruts, and other damage phenomena of semirigid base course asphalt pavement before reaching the design service life [6–9]. Therefore, whether for full-depth pavement or semirigid base pavement, it is very necessary to accurately analyze the dynamic response of pavement under vehicle load.

Most of the early studies on the dynamic response of pavement structure under the moving load of heavy vehicles used analytical and experimental methods. In recent ten years, with the advent of the high-performance computer, various numerical methods have become a very effective tool to simulate pavement dynamics and play a more and more important role. There are two commonly used numerical methods: one is to directly use the numerical method to obtain the numerical solution of dynamic response, that is, to directly discretize the difficult partial differential equations and boundary conditions into a series of algebraic equations, and convert the mathematical analysis of continuous functions into a large number of normalized discrete values for calculation. For example, Yang et al. [10] used the Galerkin method to study the dynamic response of double-layer plate on Kelvin foundation under the coupling of vehicle and pavement and analyzed the influence of vehicle

parameters on pavement vibration. The second is the finite element method. The finite element method is a popular numerical simulation method at home and abroad. Its advantage is that it can adapt to complex geometry and boundary conditions and is suitable for solving linear and nonlinear, homogeneous, and heterogeneous problems [11, 12]. Siddharthan et al. [13] proposed a model for analyzing the strain response of pavement under real wheel load based on the finite layer theory. This model can consider the dynamic change of tire grounding pressure, the complex distribution form of grounding pressure, and vehicle speed and viscoelastic properties of materials and compiled a 3D-move finite element program on this basis.

Wu and Shen [14] combined the finite element method with Newmark integral to gradually solve the motion equation and studied the dynamic response of rigid pavement under moving single degree of freedom vehicle load. Yang et al. [15] studied the dynamic response of a three-dimensional-layered foundation under train load by using the combination of three-dimensional finite element and infinite element. Hou et al. [16] applied the three-dimensional finite element method to calculate the deformation and stress of the plate on Winkler foundation under moving point load, analyzed the natural frequency and critical speed of the plate, and discussed the effects of load moving speed, plate material parameters, and foundation parameters on the deflection and stress of the plate. Li [17] established a layered three-dimensional finite element model of semirigid pavement with ANSYS as the calculation tool, studied the stress and strain distribution characteristics of semirigid pavement under vehicle moving load, and analyzed the effects of driving speed, load, and wheel braking on pavement dynamic response. Shu and Qian [18] and Shan et al. [19] studied the dynamic characteristics of pavement structure based on ADINA and ABAQUS, respectively. Pei et al. [20] established the three-dimensional finite element model of asphalt pavement under different axle types through field investigation and studied the dynamic response of asphalt pavement under different axle load distribution conditions such as single rear axle, double rear axle, and three rear axles, respectively. Liu et al. [21] analyzed the dynamic response law of asphalt pavement structure under moving load by establishing the three-dimensional finite element model of pavement structure and compiling DLOAD and UTRACLOAD subroutines. Dong et al. [22] established the finite element model of asphalt pavement based on the assumption of transverse isotropy of materials and compared and analyzed the dynamic responses of isotropic and transverse isotropic models under moving load. Huang et al. [23] analyzed the influence of structural parameters on the dynamic response of asphalt pavement and analyzed the sensitivity of pavement structural parameters in combination with an orthogonal test. Considering the random characteristics of pavement roughness, Li et al. [24] obtained the random dynamic load sequence of four degrees of freedom vehicles acting on the pavement, developed the moving random load subroutine VDLOAD based on the secondary development platform of ABAQUS finite element software, and established the finite element dynamic analysis model of the asphalt pavement structure. Based on the model, the dynamic response of asphalt pavement structure under vehicle pavement interaction is studied. Peng et al. [25] imported the humidity field values into ABAQUS through MATLAB, indicating that the distribution of moisture content of subgrade significantly affects the resilient modulus distribution of subgrade and critical response of pavement structures. Li et al. [26] proposed a constitutive model of subgrade soils to incorporate soil suction and octahedral shear stress, and the model can be applied to analyze the fatigue cracking of both subgrade and surface layers.

The objective of this research is to reveal the dynamic response law of full-depth asphalt pavement under moving load and compare it with the performance of the traditional semirigid base pavement. Five typical pavement structures are selected, including full-depth asphalt pavement and semirigid base asphalt pavement. The three-dimensional model and dynamic load model are constructed based on ABAQUS. Through the setting of the load moving belt, the subroutine is written to realize the application of moving load, and the differences of the dynamic response of different structures are analyzed. Finally, by changing the parameters of the load-related subroutine and changing the load moving speed, the variation laws of the dynamic response of five structures under different speeds are studied.

## 2. Establishment of the Dynamic Response Model

*2.1. Pavement Structures.* In order to analyze the influence of pavement structure on dynamic response, comparing the performance difference between full-depth asphalt pavement and general semirigid base asphalt pavement, five different pavement structure types are selected [27], as shown in Table 1. Structures I, II, and III in the foundation are full-depth asphalt pavement, and structures IV and V are semirigid base asphalt pavement. The thickness and materials of each structural layer of the five pavement structures are shown in Figure 1 [27], and the values of material parameters are shown in Table 1.

*2.2. Finite Element Model.* In ABAQUS software, dynamic load simulation can be realized by setting load steps and load conditions, so as to be closer to the situation when the structure is used on the real road. With the development of finite element technology, the research community has done some research on the dynamic response of multilayer pavement under moving load, but most of them focus on the research of two-dimensional models [28–30].

In the static load analysis, the two-dimensional model can reduce the model scale and reduce the grid elements to improve the operation speed and save time. However, in the dynamic load analysis, because the vehicle driving is a dynamic process, the mechanical response at a certain position of the pavement structure changes with time, so the three-dimensional modeling analysis is needed. The current road design method generally simplifies the vehicle load into the

Table 1: Relevant parameters of various pavement materials.

| Material name | Elastic modulus (MPa) | Poisson's ratio |
|---|---|---|
| SMA-13 | 1500 | 0.25 |
| AC-13 | 1450 | 0.25 |
| AC-20 | 1400 | 0.25 |
| AC-25 | 1350 | 0.25 |
| ATB-25 | 1200 | 0.40 |
| Lime-ash soil | 800 | 0.35 |
| Cement-stabilized macadam | 1600 | 0.25 |
| Low content cement-stabilized macadam | 1300 | 0.25 |
| Modified soil | 400 | 0.40 |
| Soil | 50 | 0.40 |

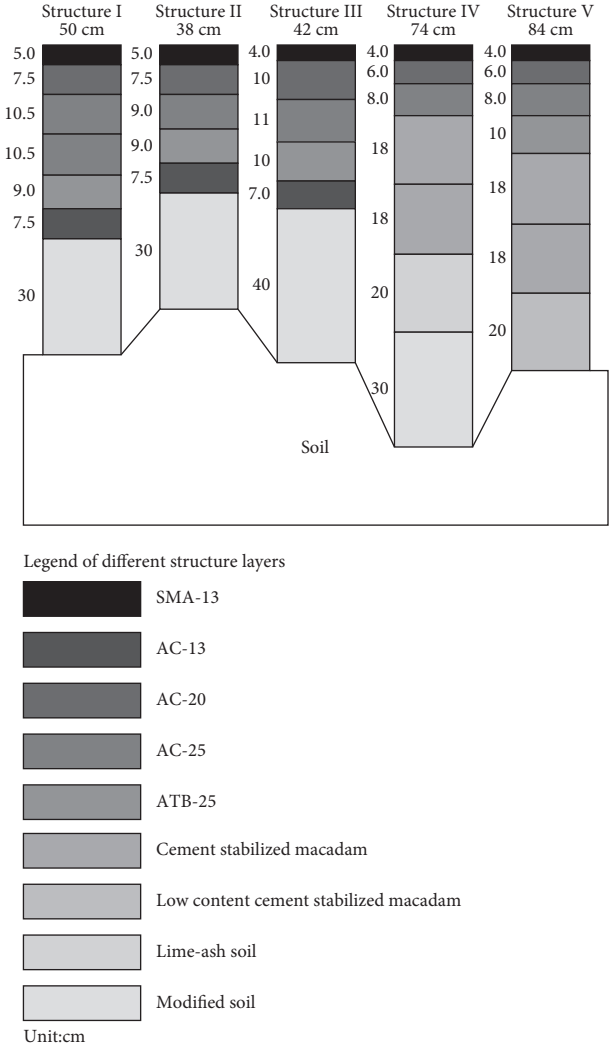


Figure 1: Pavement structure and materials.

static load. In fact, when the car is driving on the road, the road surface is affected by complex vertical and horizontal forces [31–33]. In order to simplify the problem, it is assumed that the vehicle wheel load is a vertically uniformly distributed rectangular load when the vehicle is running normally. In the braking section, it is assumed that the vehicle wheel load is uniformly distributed vertical and horizontal rectangular load.

In the calculation process, in order to realize the movement of the load, first set the load moving belt along the load moving direction. The transverse width of the moving belt along the road is the same as the applied uniformly distributed load width, and the longitudinal length of the moving belt along the road is the driving distance of the wheel load. Then, the load moving belt is subdivided into many small rectangles. As shown in Figure 2, the length of

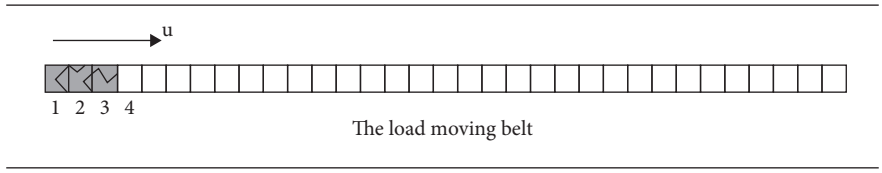


Figure 2: Load moving belt.

the small rectangle depends on the calculation accuracy and can be one third of the wheel load length.

In the initial state of wheel load, it occupies the area of three small rectangles 1, 2, and 3 in the figure. In the moving process, the load moves forward gradually along the moving belt. By setting multiple load steps, at the end of each load step, the load moves forward by a small rectangular area as a whole. For example, at the end of the first load step, the load occupies 2, 3, and 4. At the same time, in order to improve the calculation accuracy, multiple load substeps are set in each load step. For example, the middle load substep of the first load step gradually reduces the load on area 1, while the load on area 4 gradually increases, which develops in turn to achieve the effect of load movement. The moving speed of the load can be achieved by setting the time size of each load step. Since the ABAQUS foundation load setting is difficult to meet the above requirements, it is proposed to use the loading subroutine to realize the moving load. The user subroutine is written by the user according to the corresponding interface provided by ABAQUS and FORTRAN syntax. According to the needs of the problem studied, this paper compiles the subroutine VDLOAD for applying moving load. The moving speed of the load can be realized by the time of the load step in the subroutine.

The realization of dynamic load requires the establishment of a three-dimensional finite element model of the pavement structure. The cross section of the model pavement is 4 m in the transverse direction, 3 m in the depth, and 6 m in the moving direction of the load. The pavement structure is completely continuous with the five structures mentioned above. In order to reduce the influence of boundary conditions on the internal mechanical response law of pavement structure during loading, the load is applied at 1.5 m–4.5 m in the $Z$ direction of the upper surface of the model. The boundary condition is that the bottom is completely fixed, the displacement in the $X$ direction is constrained on both sides of the pavement section structure, and the displacement in the $Z$ direction is constrained before and after. The model and boundary conditions are shown in Figure 3. The upper surface of the model is the application of the load moving belt. The small rectangle on the moving belt is divided directly on the model, and then, the mesh is divided [34]. In order to facilitate calculation convergence, the grid is set more densely at the surface layer and load moving zone, while the grid at the lower soil foundation is larger. The element type adopts c3d8r, namely, eight-node linear hexahedron element, reduced integral, and hourglass control. There are 56160 units in the model, and the meshing results are shown in Figure 4.

## 3. Results and Discussion

*3.1. Time History Curve of Each Structure.* Considering the vertical uniformly distributed load, the selected calculation point of stress is the special center point directly below the wheel load. The road surface, the bottom of upper layer, the bottom of middle layer, the bottom of lower layer, the bottom of ATB layer, the bottom of AC-13 layer, and the bottom of the modified soil layer are selected, respectively, to obtain the time history curves of vertical displacement, stress, strain, and shear stress of five structures, as shown in Figure 5. Among them, due to the setting of the load step, when the load moves to the center of the model, the time is about 0.0475 s, and there are slight differences before and after different structures, which can be seen in the resulting diagram.

Through the above curve, the changes of various indexes of the selected pavement structure in the process of dynamic load can be analyzed. According to the curve change, when the time history curve time reaches about 0.04 s, the slope in the time history curve increases significantly. The reason is that the load enters the area near the center point of the model at about 0.04 s, and the load in this area has a more direct influence on the internal mechanical changes of each structural layer.

For vertical displacement, the displacement value of the road surface is the largest in each time period, and the subsequent curves of each layer gradually decrease with the increase of layer depth.

The change of vertical stress is similar to vertical displacement. When the load moves to the center, the value of vertical stress gradually increases, the change value increases near 0.04~0.06 s, and the vertical stress of each layer reaches the maximum at 0.05 s.

The variation law of vertical micro strain in each layer is slightly different. With the increase of time, the vertical micro strain at the road surface, upper layer bottom, and middle layer bottom first increases positively, decreases rapidly, and becomes negative when it reaches 0.04 s, and the image is symmetrical about the time median. The other four-layer curves first increase in the negative direction to the peak value and then decrease with the increase of time.

The longitudinal shear stress of each layer first increases with time, rapidly increases to the peak near 0.04 s, decreases to 0 at 0.05 s, and then rapidly increases to the peak in the opposite direction. The curve trend is symmetrical about the midpoint of time.

For the transverse shear stress, the change trend of time history curve of each layer is the same, which first increases

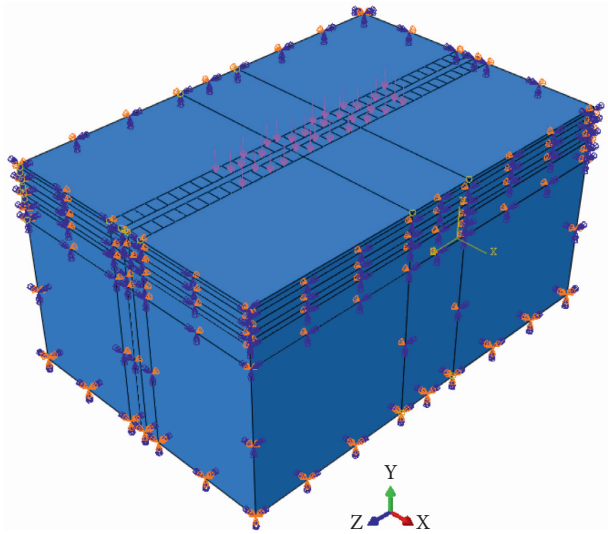


Figure 3: 3D model and boundary conditions.

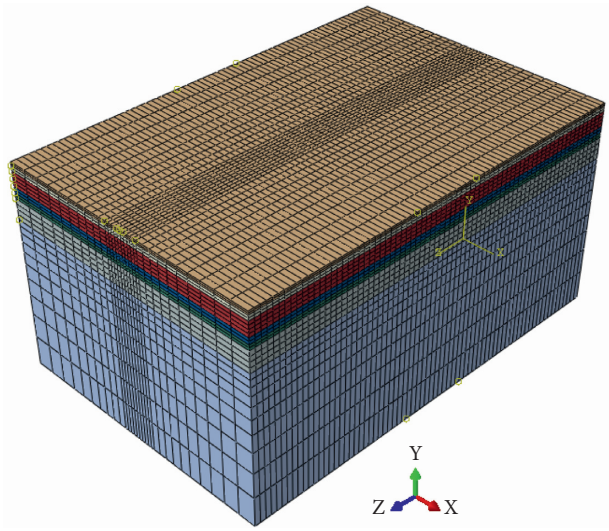


Figure 4: Grid division of the 3D model.

to the peak and then decreases, and the transverse shear stress at the bottom of the lower layer is the largest.

According to the above conclusions, the same analysis is made for the remaining four structures, and the data are extracted to obtain the time history curves of each index of the other four structures at the above positions, as shown in Figures 6–9, which are analyzed, respectively.

Comparing the time history curves of structure I and structure II, the overall law is roughly similar, but the values of each index are quite different. Compared with structure I, the maximum value of vertical displacement, vertical strain, and transverse shear stress of structure II increases, while the maximum value of vertical stress decreases, and the longitudinal shear stress changes little.

It can be seen that, compared with the first two structures, the vertical displacement time history curve of structure III has better symmetry. The vertical displacement value is also small, and the mechanical response under dynamic load is more stable. In general, the distribution of the selected indexes of the first three structures is similar, and the time history curves of the three full-depth structures have little difference.

Structure IV and structure V are two traditional semirigid structures used as the control group. Their structures are different from the first three. Cement-stabilized macadam semirigid structure layers are set at the bottom of the ATB layer. Different structures make the internal index values of the five structures have great differences. The vertical displacement value of the latter two semirigid structures decreases obviously, and the fluctuation of stress and strain also decreases. However, for structure IV and structure V, the indexes of the bottom of the middle surface layer are larger than the first three full-depth structures. Among the selected structural layers, the upper layer of each structure is quite different from the middle layer. According to other studies, the stress state of these two structural layers is relatively severe, which is the main embodiment of structural change. Because the road surface bears load directly, the values of other indicators are generally large except shear stress. Through the above analysis, it can be found that although the time history curve law of each index of each structure is different, it is not intuitive. The numerical differences need to be more intuitive compared in the follow-up research.

*3.2. Numerical Comparison of Time History Curves of Various Structures.* In order to study the different dynamic response laws among the five structures, it is necessary to compare the time history curves and index variation curves with the depth of different structures to study their variation laws. The analysis of the variation law of time history curves of different structures is reflected in the previous section. This section mainly analyzes the above results from the numerical point of view. According to the time history curve in the previous section, the maximum values of vertical displacement, vertical stress, strain, and longitudinal shear stress inside the structure appear on the road surface, and the maximum value of transverse shear stress generally appears at the bottom of the lower layer. Therefore, the time history curves of the five structures are compared according to the location of the maximum index, and the time history curves of each index on the same layer of the five structures are obtained as shown in Figure 10.

In order to more intuitively compare the different index values of the five structures in the same layer, the five pavement structures are now sorted according to different indexes. The smaller the serial number, the smaller the index value, as shown in Table 2.

In general, the semirigid base pavement has better bearing capacity under dynamic load. For the vertical displacement of road surface, the performance of full-depth asphalt pavement is worse than that of semirigid base pavement, which will be reflected as a rutting problem in practical engineering. Therefore, for full-depth pavement, a high modulus asphalt mixture should be used to reduce this adverse effect. In addition, the full-depth asphalt pavement

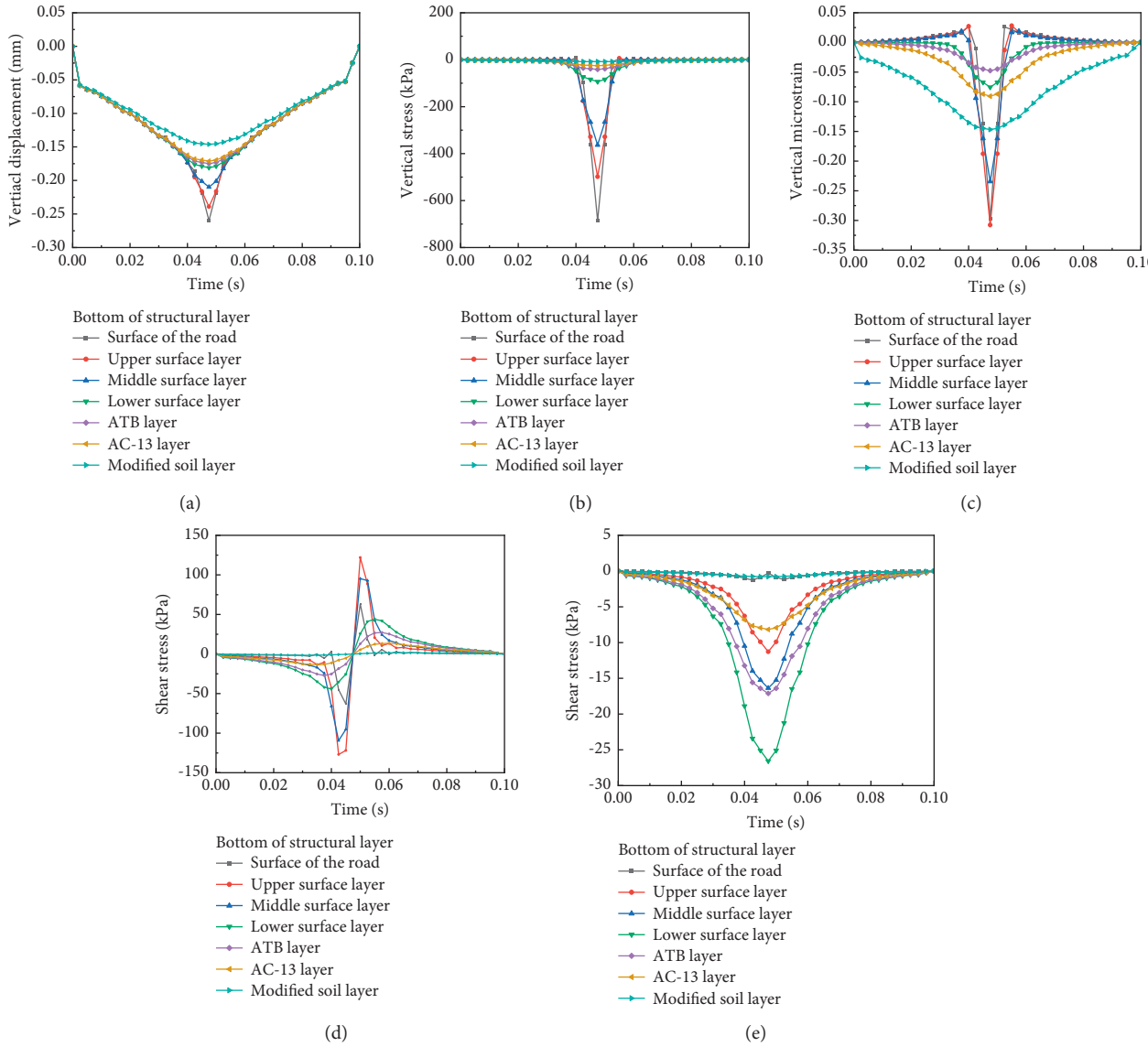


Figure 5: Time history curve of (a) vertical displacement, (b) vertical stress, (c) vertical micro strain, (d) longitudinal shear stress, and (e) transverse shear stress at each layer of structure I.

produces greater transverse shear stress under dynamic load, which means that the bottom of the lower layer is more prone to cracking. Therefore, it is necessary to set up a stress-absorbing layer to dissipate the internal stress in the design of full-depth asphalt pavement.

*3.3. Dynamic Response of Full-Depth Pavement at Different Moving Load Speeds.* In the actual use of pavement structure, the vehicle speed is often different, so it is necessary to analyze the dynamic response of pavement structure at different speeds. Structure I is selected for corresponding research. Referring to the current regulations of speed limit on expressways, it is assumed that cars are traveling at a uniform speed of 60 km/h, 72 km/h, 84 km/h, 96 km/h, 108 km/h, and 120 km/h, respectively, and then, the corresponding loads advance 1.67 m, 2 m, 2.33 m, 2.67 m, 3 m, and 3.33 m, respectively, within 0.1 s. According to the grid size, the number of grids occupied by the load within 0.1 s is 10, 12, 14, 16, 18, and 20, respectively. The simulation calculation is carried out for structure I, and the time history curves at different speeds and the curves with depth are obtained, as shown in Figures 11 and 12.

According to Figure 11, the vertical displacement of the road surface in the structure decreases with the increase of speed. When the speed is low, the vertical displacement of the road surface is large, which is also in line with the law of practical experience. As the load moves to the center, the vertical displacement of the selected point first increases, decreases near the center, and then increases; after selecting the position, the vertical displacement decreases slightly and then increases, and finally, the load moves back to the selected point, and the vertical displacement also decreases. The change of load speed basically has no effect on the

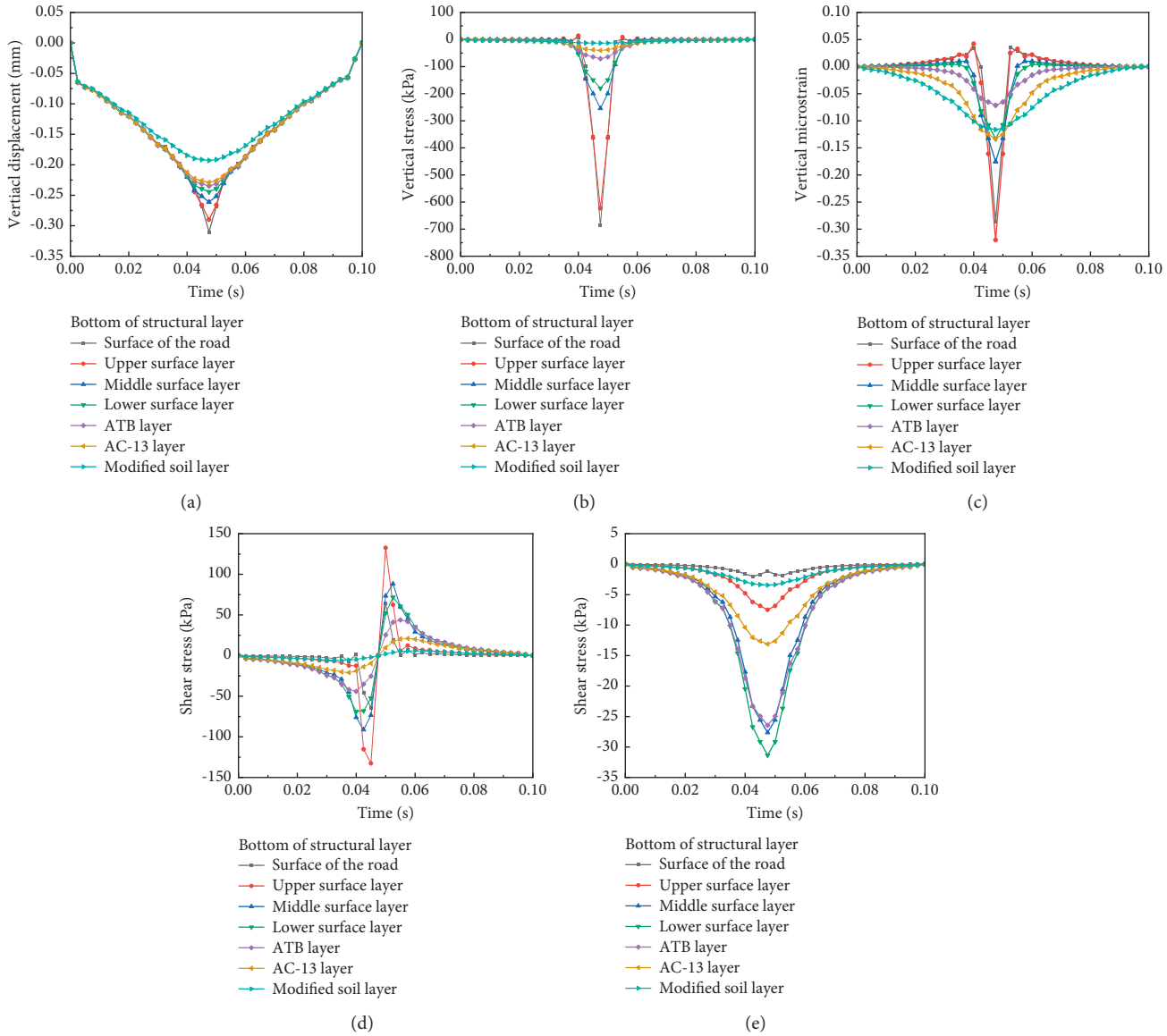


Figure 6: Time history curve of (a) vertical displacement, (b) vertical stress, (c) vertical micro strain, (d) longitudinal shear stress, and (e) transverse shear stress at each layer of structure II.

vertical stress and vertical strain of the road surface. The curve heights of different speeds coincide, and the values are similar, but the time to reach the maximum value is slightly different. This is the reason for the analysis step, not the effect of speed. The regularity of the longitudinal shear stress time history curve of road surface under different speeds is not obvious. Due to the large fluctuation of shear stress, the maximum value changes little with the speed, and the shear stress value is large at 72 km/h, 96 km/h, and 108 km/h. For the longitudinal shear stress, the value increases with the increase of speed. When the speed is 120 km/h, the longitudinal shear stress reaches 120 kPa.

Figure 12 shows the change of each index with depth on the taken path at different speeds. It can be seen from the figure that on the selected path, the vertical displacement increases with the increase of load speed, and the variation laws of different speed curves are basically the same. When the depth reaches 3 m, the vertical displacement of each curve is 0. The coincidence degree of vertical stress curve with depth under different speeds is higher, and the stress with high speed is slightly larger. The vertical micro strain increases with depth in the upper layer, then decreases with depth, and fluctuates after entering the base layer, which is consistent with the above law. With the increase of velocity, the maximum value of vertical micro strain decreases slightly, but the difference between the maximum value and the minimum value is less than 5%. Because the longitudinal shear stress fluctuates with depth at the selected position, it is difficult to compare its maximum value, but the overall law is similar. The variation law of transverse shear stress with depth under different speeds is the same, which increases with depth in the upper layer, and then decreases with depth.

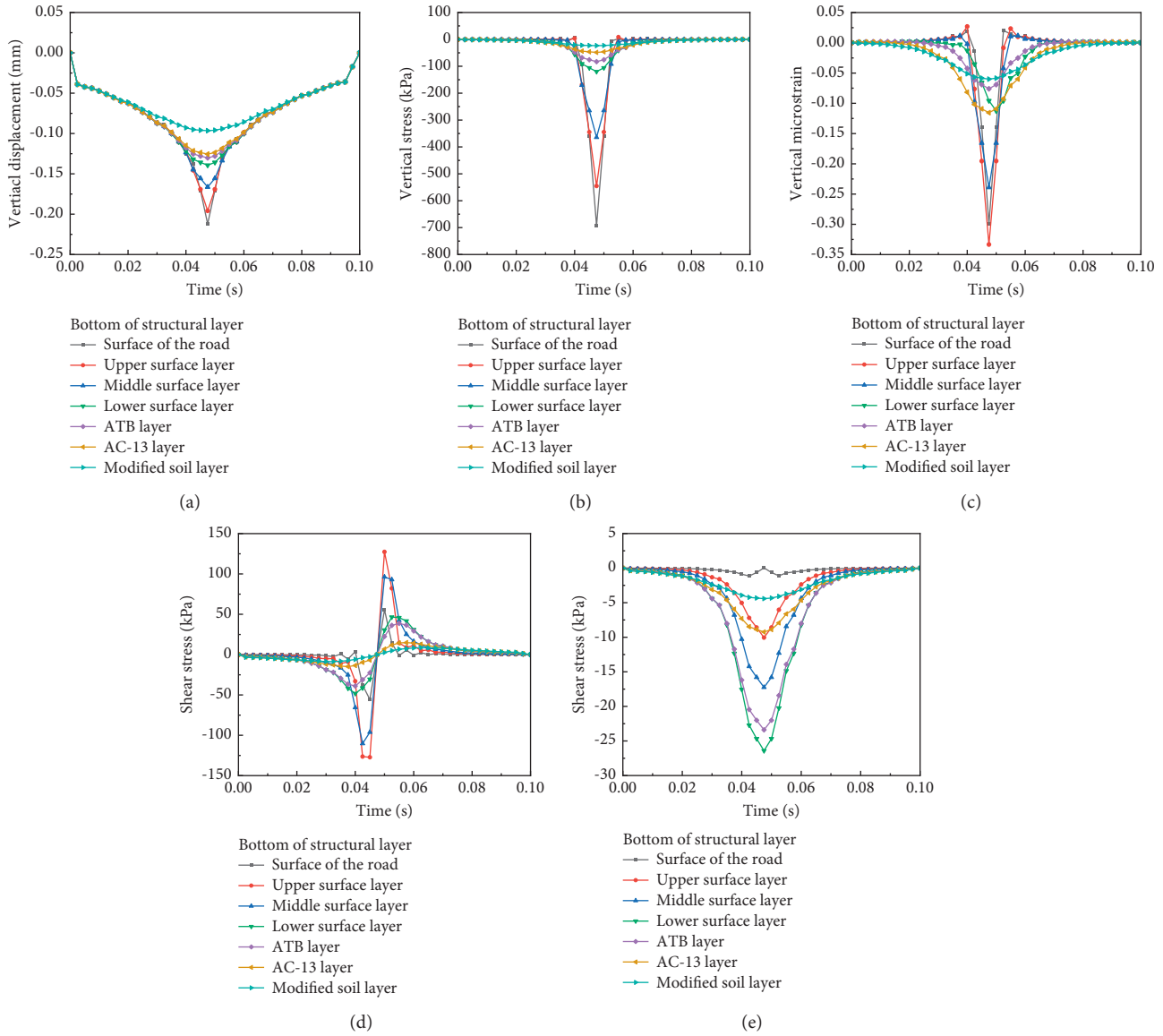


Figure 7: Time history curve of (a) vertical displacement, (b) vertical stress, (c) vertical micro strain, (d) longitudinal shear stress, and (e) transverse shear stress at each layer of structure III.

When the depth is 3 m, the value of each curve is 0. According to the maximum value at the bottom of the upper layer, the value of transverse shear stress increases with the increase of velocity.

According to the above conclusions, the increase of speed will increase the vertical displacement at the wheel load action point, but for the whole structure, the increase of speed will reduce the vertical displacement at other positions in the process. The vertical stress-strain and longitudinal shear stress change little and can be ignored. However, the increase of speed increases the transverse shear stress of the pavement. It can be considered that the transverse tensile

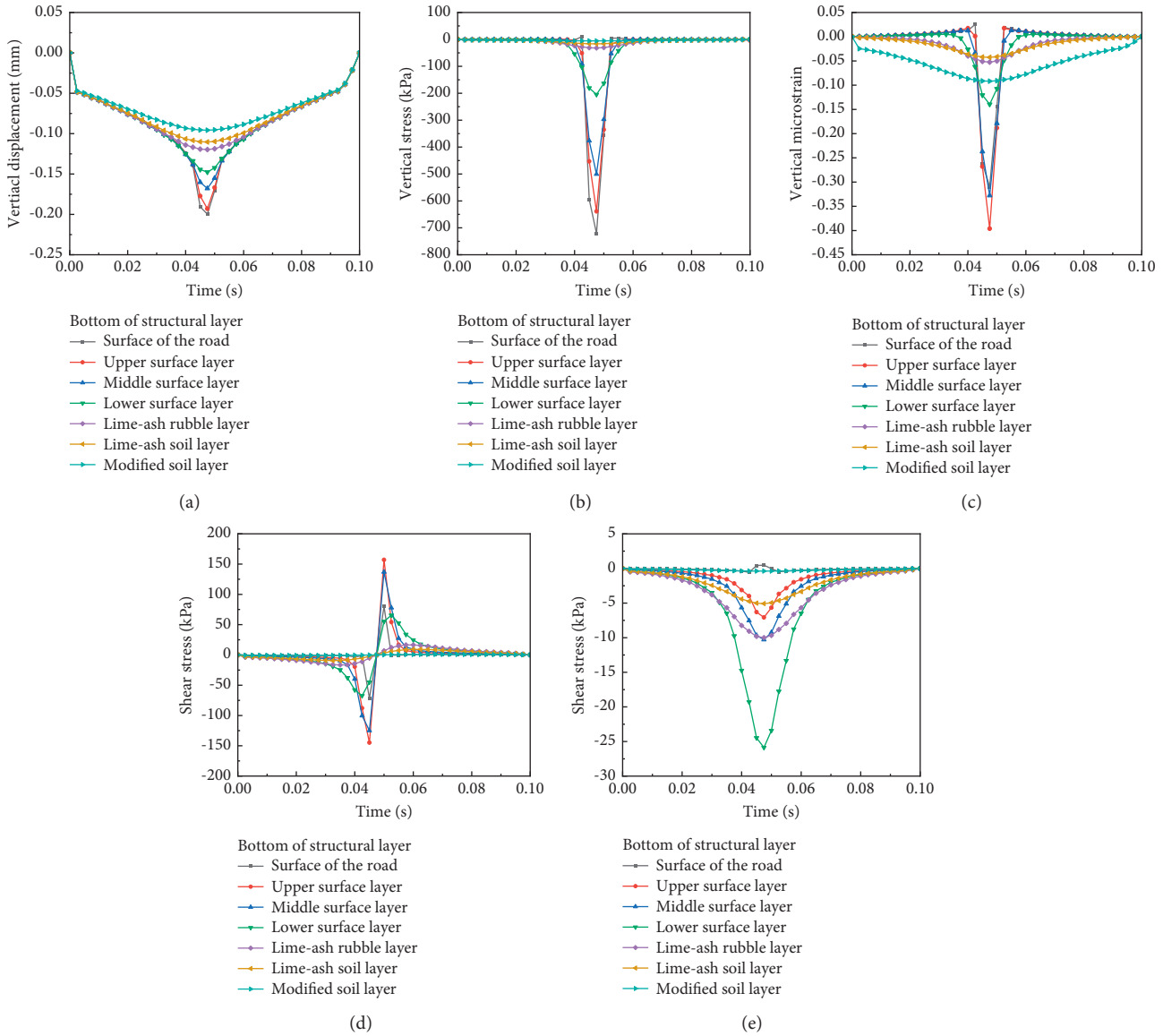


Figure 8: Time history curve of (a) vertical displacement, (b) vertical stress, (c) vertical micro strain, (d) longitudinal shear stress, and (e) transverse shear stress at each layer of structure IV.

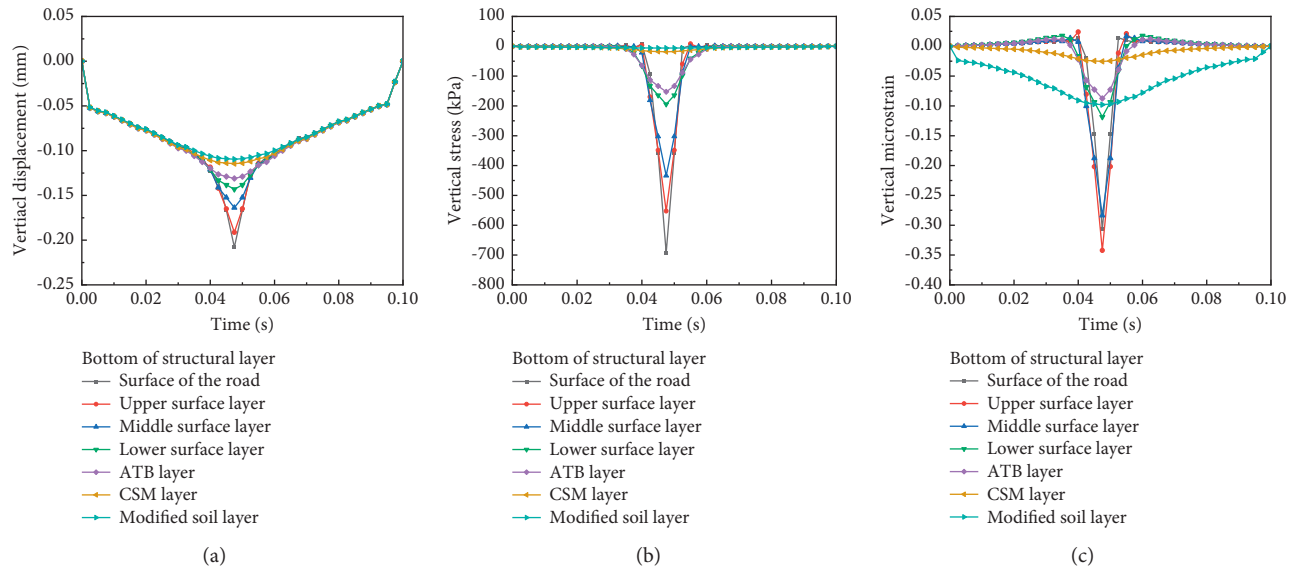


Figure 9: Continued.

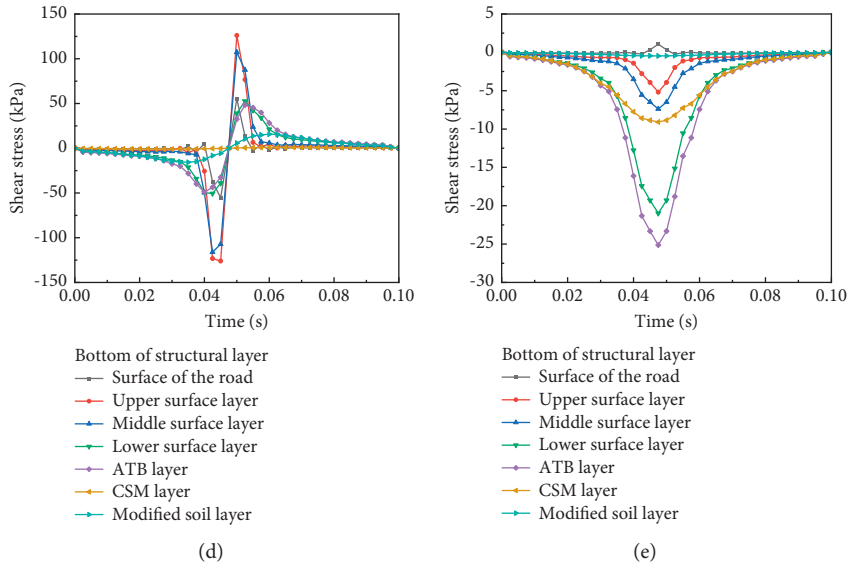


Figure 9: Time history curve of (a) vertical displacement, (b) vertical stress, (c) vertical micro strain, (d) longitudinal shear stress, and (e) transverse shear stress at each layer of structure V.

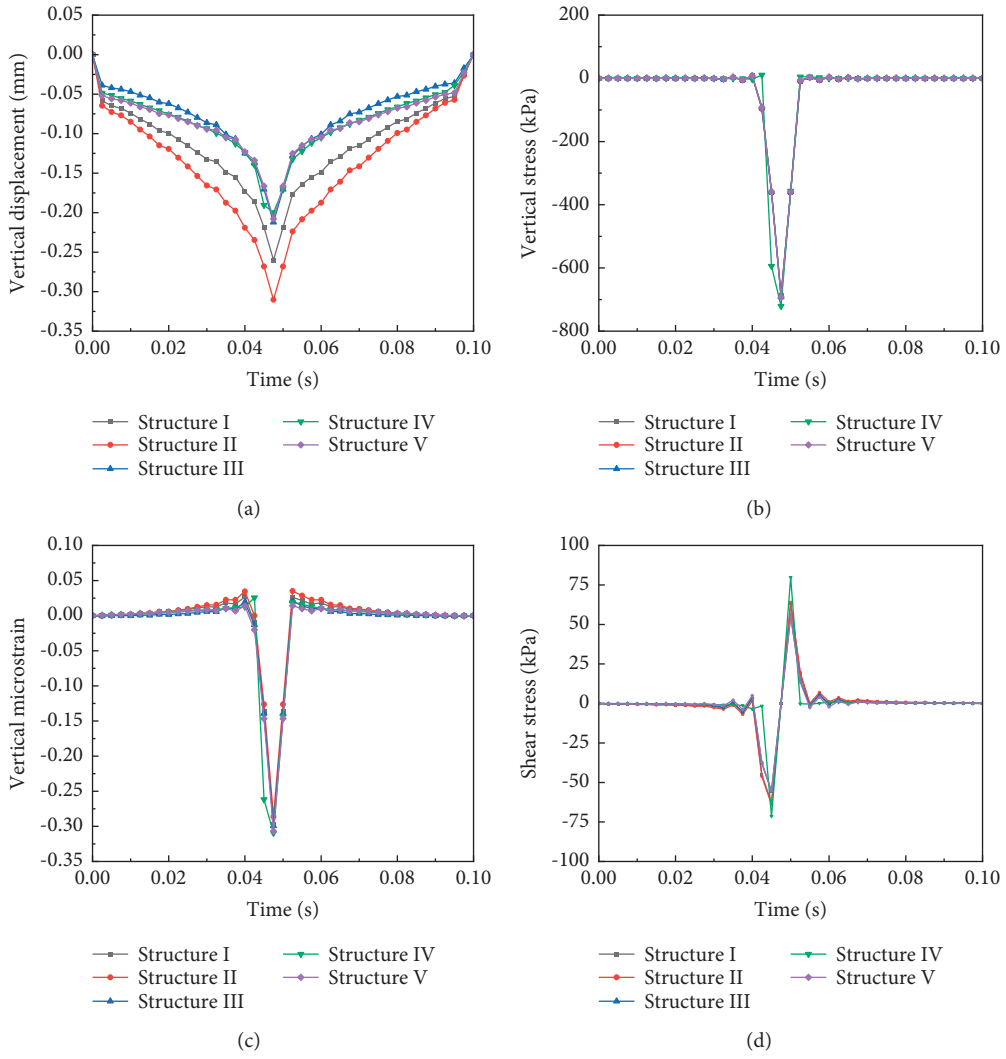


Figure 10: Continued.

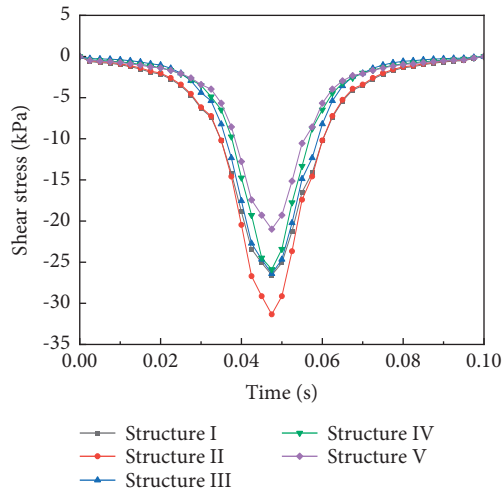


(e)

Figure 10: Time history curve of each index of five structures. (a) Time history curve of vertical displacement of the road surface. (b) Time history curve of vertical stress of road surface. (c) Time history curve of the vertical micro strain of road surface. (d) Time history curve of longitudinal shear stress of road surface. (e) Time history curve of transverse shear stress at the bottom of the lower surface layer.

Table 2: Ranking of indicators of five structures.

| | Full-depth asphalt pavement | | | Semirigid base pavement | |
|---|---|---|---|---|---|
| | I | II | III | IV | V |
| Vertical displacement | 4 | 5 | 3 | 1 | 2 |
| Vertical micro strain | 4 | 1 | 3 | 5 | 2 |
| Longitudinal shear stress | 3 | 4 | 2 | 5 | 1 |
| Transverse shear stress | 4 | 5 | 3 | 2 | 1 |

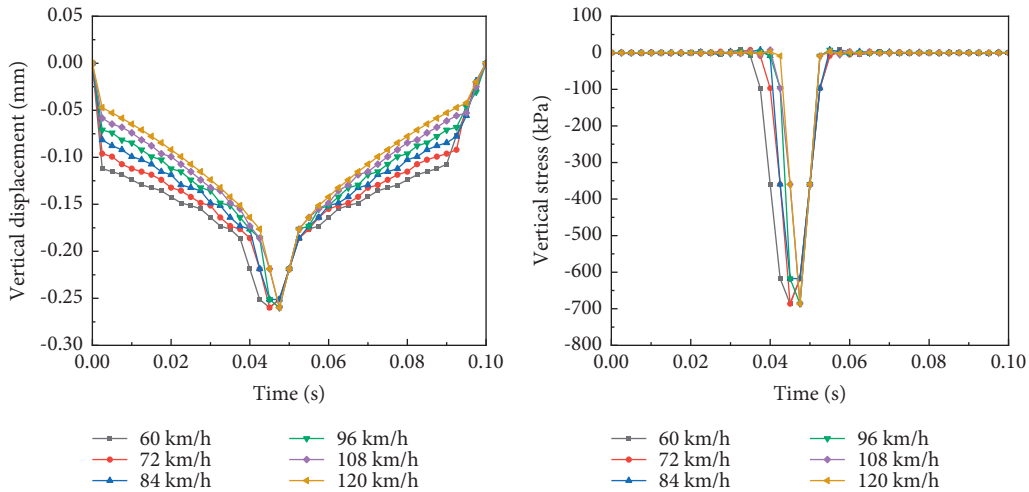


(a) (b)

Figure 11: Continued.

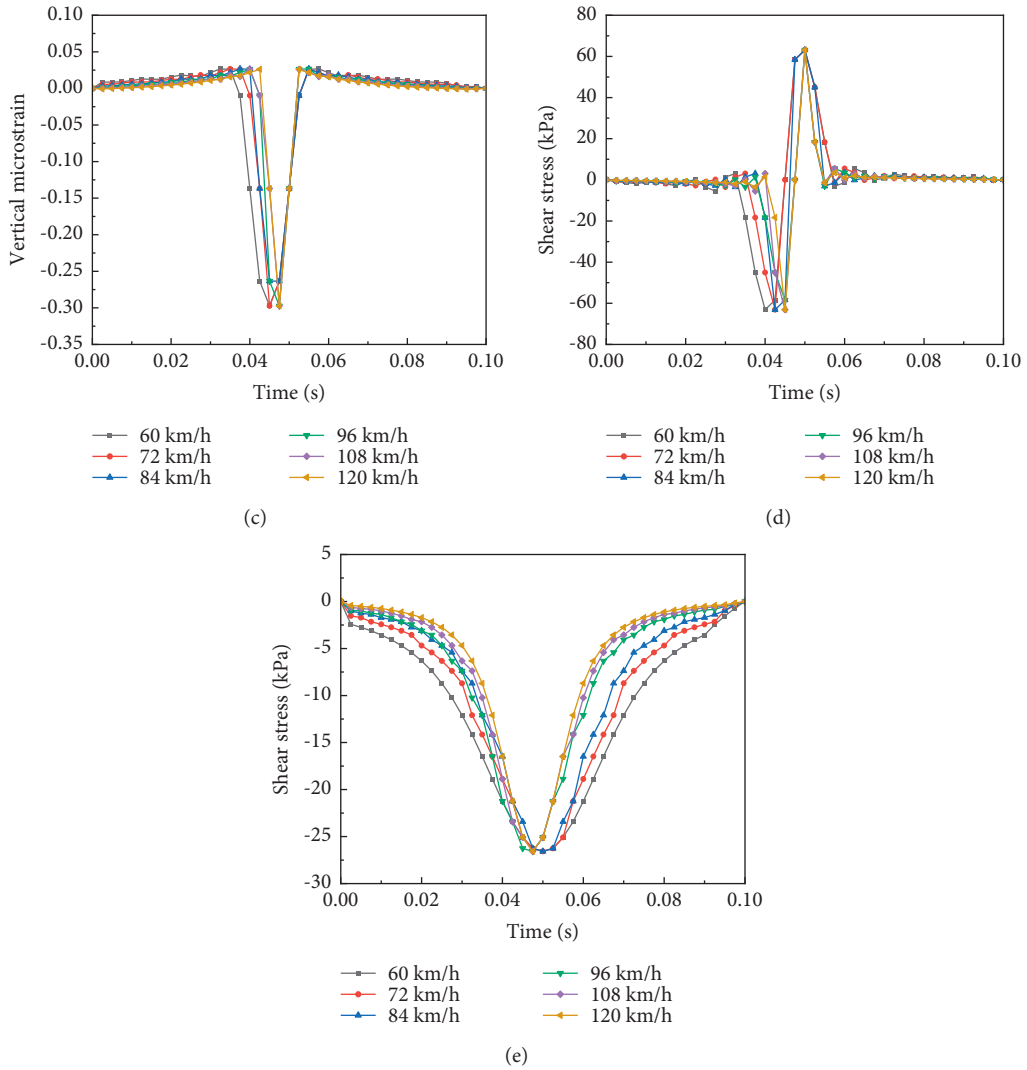


Figure 11: Time history curve of each index of structure I. (a) Time history curve of vertical displacement of road meter at different speeds. (b) Time history curve of vertical stress of road surface at different speeds. (c) Vertical micro strain time history curves of road meters at different speeds. (d) Time history curve of longitudinal shear stress of road surface at different speeds. (e) Time history curve of transverse shear stress at layer under different speeds.

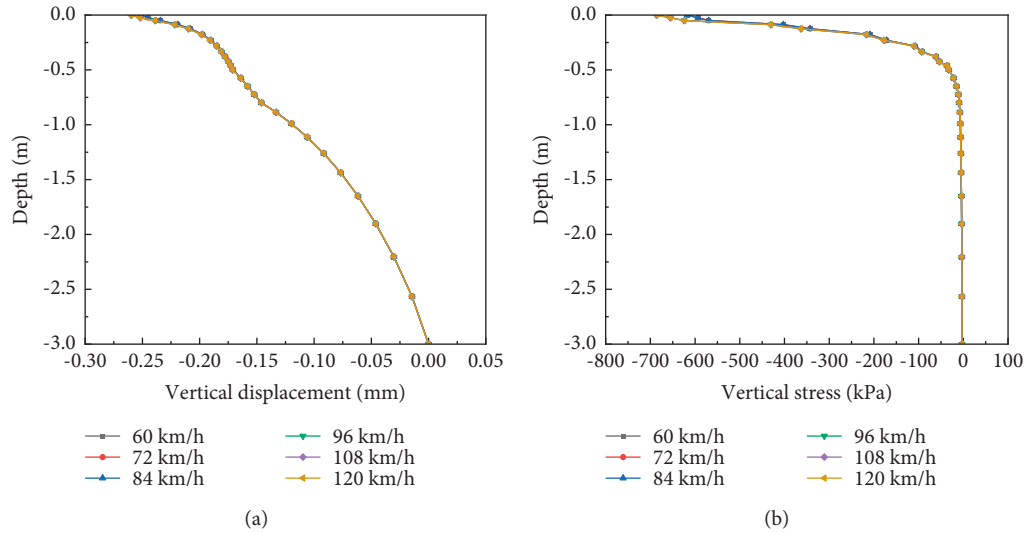


Figure 12: Continued.

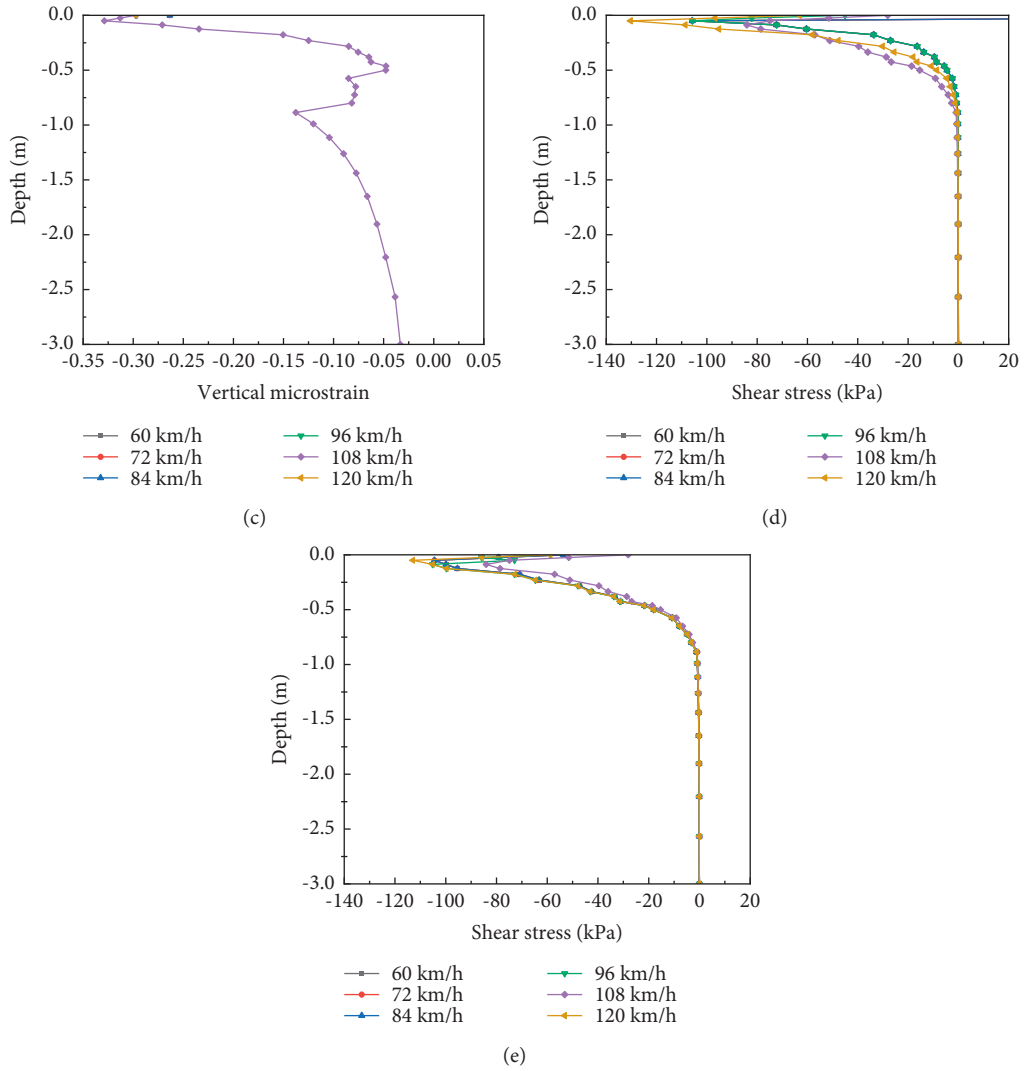


Figure 12: (a) Variation of vertical displacement with depth at different speeds. (b) Variation of vertical stress with depth at different speeds. (c) Variation of vertical micro strain with depth at different speeds. (d) Variation of longitudinal shear stress with depth at different speeds. (e) Variation of transverse shear stress with depth at different speeds.

stress at the bottom of each layer increases, which means that the pavement is more prone to longitudinal cracks.

## 4. Conclusion

(1) In the time history curve analysis of different positions of each structural layer, compared with full-depth asphalt pavement, the vertical displacement of the road surface of the semirigid base pavement is significantly reduced, and the stress-strain fluctuation is also small. However, for the middle surface layer, the displacement, vertical stress, and shear stress of semirigid base pavement are greater than those of full-depth pavement, which is also the embodiment of full-depth pavement in reducing rutting disease in dynamic response.

(2) In the comparison of time history curves of different structures, the vertical stress and strain of the five structures have little difference, and the transverse shear stress at bottom of the upper layer of full-depth pavement is greater than that of semirigid base pavement. Full-depth asphalt pavement should pay more attention to the cracking resistance of the upper layer mixture, which will directly affect the pavement performance and surface life.

(3) In the dynamic response analysis under different vehicle speeds, the vertical displacement of the road surface is large when the speed is low, which is

related to the load action time. The increase of speed will be accompanied by the increase of transverse shear stress at the bottom of the structural layer, and the pavement is more prone to longitudinal crack. The crack development can be restrained by setting a stress-absorbing layer in the pavement structure.

(4) The bearing capacity of semirigid base pavement is better, but the longitudinal shear stress in structure IV is the worst, which also indicates that the bottom of the pavement is prone to cracking. Combined with the shrinkage cracking of the base layer, it is detrimental to the pavement life. The full-depth pavement needs to consider the thickness and material design of each structural layer to make up for the bearing capacity defects and obtain longer service life. In practical application, the selection of pavement structure should take traffic conditions and service life into consideration.

## Data Availability

The data used to support the findings of this study are included within the article.

## Conflicts of Interest

The authors declare that they have no conflicts of interest.

## Acknowledgments

This study was supported by the National Natural Science Foundation of China (51808016 and 52078018) and the Transportation Science and Technology Project of Shandong Province (2020B25).

## References

[1] D. M. Mrawra and J. Luca, "Thermal properties and transient temperature response of full-depth asphalt pavements," *Transportation Research Record-series*, vol. 1809, pp. 160–171, 2002.

[2] H. Ceylan, A. Guclu, E. Tutumluer, and M. R. Thompson, "Backcalculation of full-depth asphalt pavement layer moduli considering nonlinear stress-dependent subgrade behavior," *International Journal of Pavement Engineering*, vol. 6, no. 3, pp. 171–182, 2005.

[3] O. Pekcan, E. Tutumluer, and J. Ghaboussi, "SOFTSYS for backcalculation of full-depth asphalt pavement layer moduli," *Erol Tutulumluer*, vol. 1, pp. 679–687, 2009.

[4] E. Kassem, L. Walubita, T. Scullion, E. Masad, and A. Wimsatt, "Evaluation of full-depth asphalt pavement construction using X-ray computed tomography and ground penetrating radar," *Journal of Performance of Constructed Facilities*, vol. 22, no. 6, pp. 408–416, 2008.

[5] L. Johanneck and S. Dai, "Responses and performance of stabilized full-depth reclaimed pavements at the Minnesota road research facility," *Transportation Research Record*, vol. 2368, pp. 114–125, 2013.

[6] A. Braham, "Comparing life-cycle cost analysis of full-depth reclamation versus traditional pavement maintenance and rehabilitation strategies," *Transportation Research Record*, vol. 2573, pp. 49–59, 2016.

[7] Y. D. Wang, J. Jeong, and Y. R. Kim, "Comparison of treatment timing between aggregate base and full-depth asphalt roads," *Journal of Transportation Engineering Part B-Pavements*, vol. 146, no. 4, 2020.

[8] M. Guo, H. Liu, Y. Jiao et al., "Effect of WMA-RAP technology on pavement performance of asphalt mixture: a state-of-the-art review," *Journal of Cleaner Production*, vol. 266, Article ID 121704, 2020.

[9] X. Yan, P. An, W. Wu, L. Wang, and J. Wei, "feasibility study on application of full depth asphalt pavement in national trunk road," *6th International Conference on Environmental Science and Civil Engineering*, vol. 455, 2020.

[10] S. P. Yang, L. S. L. Y. Engineering, S. R. Institute, S. Li, and Y. Lu, "Dynamics of vehicle-pavement coupled system based on a revised flexible roller contact tire model," *Science in China(Series E:Technological Sciences)*, vol. 52, 2009.

[11] Y. S. Yao, J. Li, J. J. Ni, C. Liang, and A. Zhang, "Effects of gravel content and shape on shear behaviour of soil-rock mixture: experiment and DEM modelling," *Computers and Geotechnics*, vol. 141, 2022.

[12] J. H. Zhang, H. S. Fan, S. P. Zhang, and J. Zheng, "Time-domain elasto-dynamic model of a transversely isotropic, layered road structure system with rigid substratum under a FWD load," *Road Materials and Pavement Design*, 2021.

[13] R. V. Siddharthan, P. E. Sebaaly, M. El-Desouky, D. Strand, and D. Huft, "Heavy off-road vehicle tire-pavement interactions and response," *Journal of Transportation Engineering*, vol. 131, no. 3, pp. 239–247, 2005.

[14] C.-P. Wu and P.-A. Shen, "Dynamic analysis of concrete pavements subjected to moving loads," *Journal of Transportation Engineering*, vol. 122, no. 5, pp. 367–373, 1996.

[15] Y. B. Yang, H. H. Hung, and D. W. Chang, "Train-induced wave propagation in layered soils using finite/infinite element simulation," *Soil Dynamics and Earthquake Engineering*, vol. 23, no. 4, pp. 263–278, 2003.

[16] Y. Hou, S. P. Sun, and Z. Y. Guo, "Dynamic response sensitivity analysis of plate on elastic foundation subjected to moving point loads," *Journal of Tongji University*, vol. 1, pp. 31–35, 2003.

[17] X. Y. Li, *Finite Analysis of Concrete Bridge Deck Pavement at Coupling Effect*, Dalian University of Technology, Dalian, Liaoning, China, 2012.

[18] F. M. Shu and Z. D. Qian, "Analysis on dynamic response of asphalt pavement under moving load," *Journal of Transportation Engineering and Information*, vol. 5, no. 3, pp. 90–95, 2007.

[19] J. S. Shan, X. M. Huang, and G. Y. Liao, "Dynamic response analysis of pavement structure under moving load," *Journal of Highway and Transportation Research and Development*, vol. 24, no. 1, pp. 10–13, 2007.

[20] J. Z. Pei, H. Wu, Y. Chen, and B. Wang, "Dynamic response characteristics of asphalt pavement under multi-axle moving load," *China Journal of Highway and Transport*, vol. 24, no. 5, pp. 30–35, 2011.

[21] X. Y. Liu, C. J. Shi, and S. J. Chen, "A theory research of asphalt pavement dynamic response under vehicle random stimulation," *Applied Mechanics and Materials*, vol. 105, no. 6, pp. 13–19, 2011.

[22] Z. J. Dong, M. H. Liu, H. Zheng, and X. Gong, "Dynamic mechanical analysis of asphalt pavement based on cross-isotropic properties," *China Journal of Highway and Transport*, vol. 25, no. 5, pp. 18–23, 2012.

[23] B. Huang, Y. Wu, C. F. Ai, and Z. F. Zhou, "Influence of structural parameters on dynamic response of asphalt pavement," *Journal of Highway and Transportation Research and Development*, vol. 30, no. 9, pp. 8–12, 2013.

[24] Q. Li, J. Q. Liu, and H. Liu, "Random dynamic response analysis of asphalt pavement based on the vehicle-pavement interaction," *Applied Mechanics and Materials*, vol. 744-746, pp. 1288–1297, 2015.

[25] J. H. Peng, J. H. Zhang, J. Li, J. Yao, and A. Zhang, "Modeling humidity and stress-dependent subgrade soils in flexible pavements," *Computers and Geotechnics*, vol. 120, 2020.

[26] J. Li, J. L. Zheng, Y. S. Yao, J. Zheng, and J. Peng, "Numerical method of flexible pavement considering moisture and stress sensitivity of subgrade soils," *Advances in Civil Engineering*, vol. 2019, Article ID 7091210, 10 pages, 2019.

[27] F. J. Hou, T. Li, X. Li, Y. Li, and M. Guo, "Research on the anti-reflective cracking performance of a full-depth asphalt pavement," *Sustainability*, vol. 13, 2021.

[28] J. Y. Liu, L. J. Zhang, B. Kou, and P. Shen, "The environment-friendly high-elasticity asphalt mixture using as stress absorbing layer," *Advanced Materials Research*, vol. 490-495, pp. 3753–3761, 2012.

[29] C. Baek, "Performance evaluation of fiber-reinforced, stress relief asphalt layers to suppress reflective cracks," *Applied Sciences*, vol. 10, no. 21, p. 7701, 2020.

[30] J. Z. Tan, J. G. Wei, C. Pan, and K. X. Huang, "Shear stress calculation of rubber asphalt overlay and stress-absorbing layer," in *Proceedings of the 2016 International Conference on Civil, Architecture and Environmental Engineering*, pp. 189–193, CRC Press/Balkema, Taipei, Taiwan, 2016.

[31] R. Pan and Y. M. Li, "Effect of warm mix rubber modified asphalt mixture as stress absorbing layer on anti-crack performance in cold region[J]," *Construction and Building Materials*, vol. 251, 2020.

[32] K. Emad, W. Lubinda, S. Tom, M. Eyad, and W. Andrew, "Evaluation of full-depth asphalt pavement construction using X-ray computed tomography and ground penetrating radar," *Journal of Performance of Constructed Facilities*, vol. 22, no. 6, pp. 408–416, 2008.

[33] J. Luke and D. Shongtao, "Responses and performance of stabilized full-depth reclaimed pavements at the Minnesota road research facility," *Transportation Research Record*, vol. 2368, no. 1, pp. 114–125, 2013.

[34] B. Andrew, "Comparing life-cycle cost analysis of full-depth reclamation versus traditional pavement maintenance and rehabilitation strategies," *Transportation Research Record*, vol. 2573, no. 1, pp. 49–59, 2016.